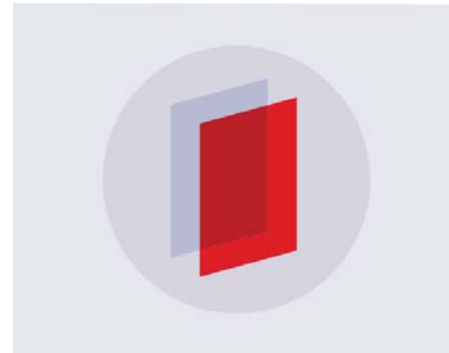
#### **PAPER**

### Structural and magnetic properties of bulk Mn<sub>2</sub>PtSn

To cite this article: J Herran et al 2018 J. Phys.: Condens. Matter 30 475801

View the article online for updates and enhancements.



# IOP ebooks™

Bringing you innovative digital publishing with leading voices to create your essential collection of books in STEM research

Start exploring the collection - download the first chapter of every title for free.

J. Phys.: Condens. Matter 30 (2018) 475801 (6pp)

## Structural and magnetic properties of bulk Mn<sub>2</sub>PtSn

J Herran<sup>1</sup>, S Prophet<sup>2</sup>, Y Jin<sup>3,4</sup>, S Valloppilly<sup>4</sup>, P R Kharel<sup>4,5</sup>, D J Sellmyer<sup>3,4</sup> and P V Lukashev<sup>2</sup>

- Department of Chemistry and Biochemistry, University of Northern Iowa, Cedar Falls, IA 50614, United States of America
- Department of Physics, University of Northern Iowa, Cedar Falls, IA 50614, United States of America
- <sup>3</sup> Department of Physics and Astronomy, University of Nebraska, Lincoln, NE 68588,

United States of America

- <sup>4</sup> Nebraska Center for Materials and Nanoscience, University of Nebraska, Lincoln, NE 68588, United States of America
- Department of Physics, South Dakota State University, Brookings, SD 57007, United States of America

E-mail: pavel.lukashev@uni.edu

Received 26 July 2018, revised 3 October 2018 Accepted for publication 5 October 2018 Published 31 October 2018



#### **Abstract**

Interplay between structural and magnetic order parameters is one of the key mechanisms of tuning properties of materials intended for device applications in spintronics. Here, using density functional calculations, we study combined effects of tetragonal distortion and noncollinear magnetic order in Mn<sub>2</sub>PtSn. We show that this material has two energetically close energy minimums corresponding to tetragonal lattice. In one of these phases, Mn<sub>2</sub>PtSn exhibits ferrimagnetic order with nearly fully compensated total magnetic moment, while in the other phase that corresponds to the lowest energy, a non-collinear magnetic arrangement emerges, with very large canting angle of the Mn local magnetic moments. The non-collinear alignment is explained through the interplay of exchange couplings between nearest and next nearest neighbor Mn atoms. Results are compared with those reported in recent literature, both experimental and theoretical.

Keywords: non-collinear magnetism, Heusler alloys, DFT calculations

(Some figures may appear in colour only in the online journal)

#### 1. Introduction

Control and tuning of magnetic degrees of freedom [1] is one of the fundamental ingredients of the field of spintronics. Practical applications include the spin-transfer-torque (STT)based magnetic random-access memory [2-6], magnetic tunnel junctions [7–10], spin injection [11–13], etc. Although many materials have been studied as potential candidates for applications in spintronics, Heusler alloys attract a special attention for their abundance in nature, and most importantly because they retain their magnetic properties well above room temperature [14–16].

While many Heusler alloys crystallize in cubic symmetry, some of these materials also exhibit tetragonal structure. In fact, Faleev et al recently performed series of density functional calculations, which indicate that some 150  $X_2YZ$ Heusler compounds are tetragonal at zero temperature [17]. This may be appealing for practical applications, as tetragonal distortion may result in emergence of magnetocrystalline anisotropy, which is absent by symmetry in cubic systems.

Magnetism in Heusler alloys has been extensively studied for many decades. Ferromagneric [18, 19], antiferromagnetic [20, 21], ferrimagnetic [22, 23], and more recently non-collinear alignment [24, 25] of magnetic moments have been

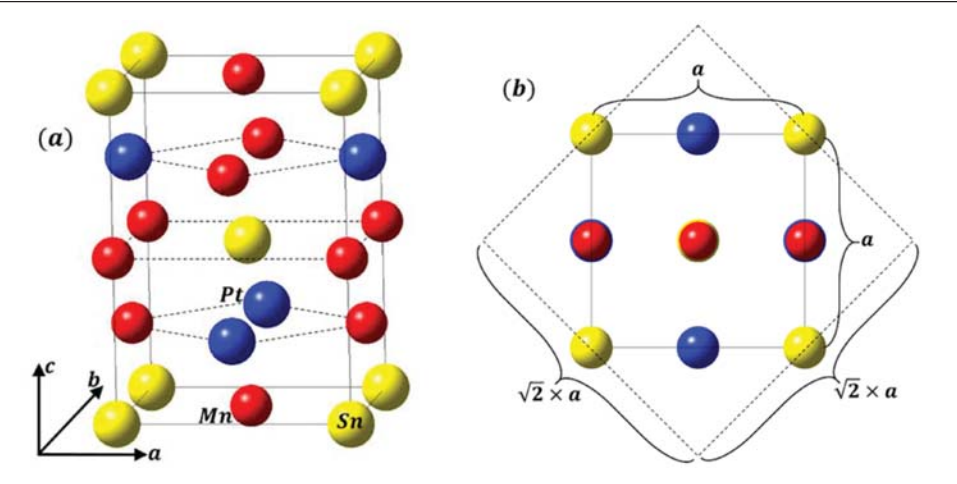
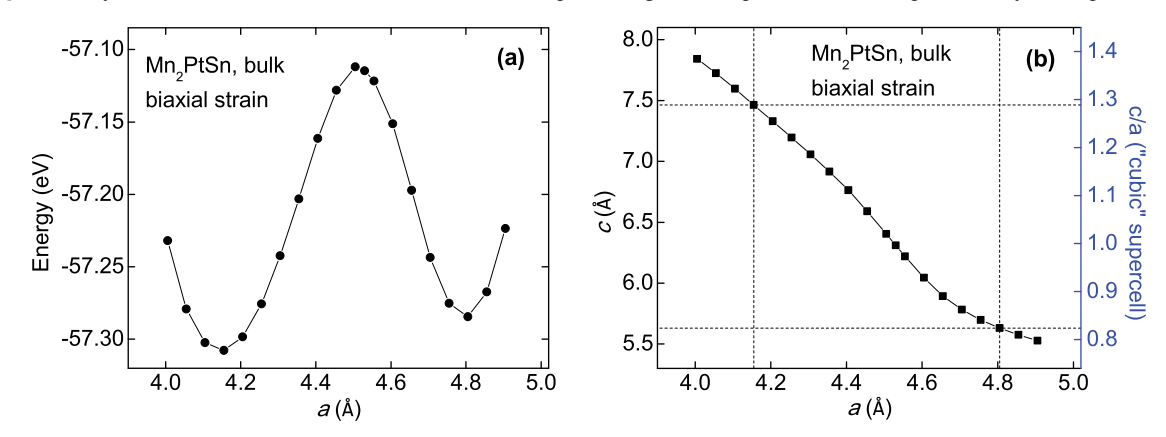


Figure 1. Crystal structure of Mn<sub>2</sub>PtSn: side view (left), and top view (right). Red sphere—Mn, blue sphere—Pt, yellow sphere—Sn.



**Figure 2.** (a) Energy, and (b) out-of-plane lattice constant versus in-plane lattice constant of bulk Mn<sub>2</sub>PtSn under biaxial strain. Dashed lines indicate lattice constants corresponding to energy minimums. The right axis in (b) shows calculated c/a ratio for the cubic supercell (see figure 1(b)).

reported. The non-collinear structure is usually considered more 'exotic' due to its relatively rare occurrence and somewhat unstable nature, e.g. it can be destroyed by temperature. Yet, it presents additional possibilities for control of magnetism, which are either absent or more difficult to attain in collinear arrangements. For example, non-collinear magnets can be used in spin valves [26], STT-based applications [27], and molecular spintronics [28].

This work is focused on Mn<sub>2</sub>PtSn Heusler material, and has two main incentives. First, according to recent experimental findings, Mn<sub>2</sub>PtSn exhibits tetragonal symmetry [29, 30]. Second, according to recent reports, Mn<sub>2</sub>PtSn and/or similar materials can also exhibit non-collinear magnetic order [24, 29, 30]. In particular, in their recent work, Meshcheriakova *et al* reported that Mn<sub>2</sub>RhSn exhibits an interplay between ferrimagnetic and non-collinear arrangement of Mn magnetic moments, with a large canting angle for the latter [24]. Here, we perform density functional calculations of bulk Mn<sub>2</sub>PtSn to analyze its structural and magnetic properties. In particular, we show how these properties can be tuned by biaxial strain. The rest of the paper is organized as follows. Section 2 outlines the computational methods. Structural and

magnetic properties of Mn<sub>2</sub>PtSn are reported in section 3. In section 4, we analyze the results, and we conclude the paper in section 5.

#### 2. Computational methods

We perform density functional calculations of bulk  $Mn_2PtSn$ , using the projector augmented-wave method [31], implemented in the Vienna *ab initio* simulation package [32] within the generalized-gradient approximation [33]. The integration method [34] with a 0.05 eV width of smearing is used, along with the plane-wave cut-off energy of  $500 \, \text{eV}$  and energy convergence criteria of  $10^{-2} \, \text{meV}$  for atomic relaxation (resulting in the Hellmann–Feynman forces being less than  $0.005 \, \text{eV}$  Å $^{-1}$ ), and  $10^{-3} \, \text{meV}$  for the total energy and electronic structure calculations. A k-point mesh of  $12 \times 12 \times 8$  is used for the Brillouin-zone integration (for atomic relaxations we used a smaller mesh of  $6 \times 6 \times 4$ ). An 8-atom cell  $Mn_4Pt_2Sn_2$  is used for all calculations, with the periodic boundary condition imposed. Crystal structures (figures 1 and 3) are visualized using the MedeA® software environment [35].

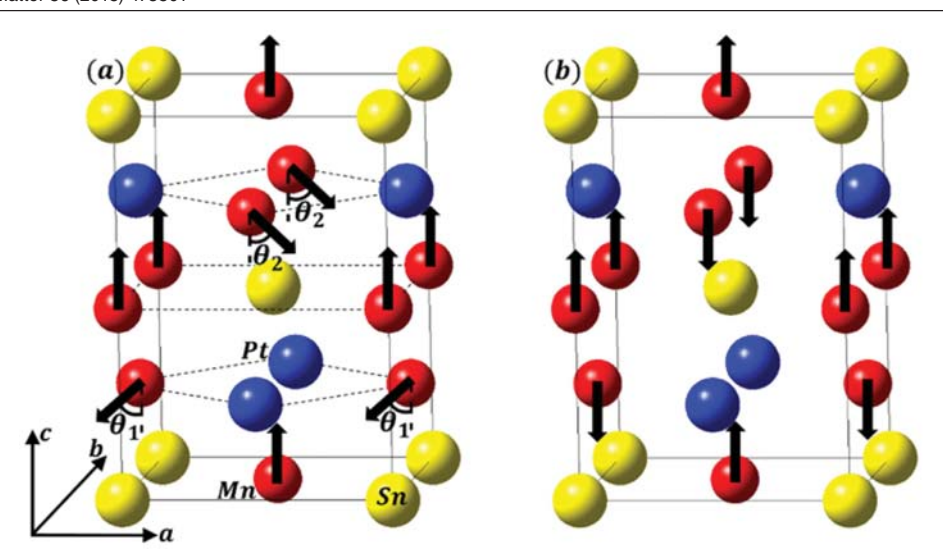


Figure 3. Non-collinear (a) and antiferromagnetic (b) arrangement of magnetic moments in bulk  $Mn_2PtSn$ . Solid black arrows indicate directions of the Mn magnetic moments.

#### 3. Results

#### 3.1. Crystal structure

We start our calculations with the initial atomic arrangement shown in figure 1. The structure is based on our recent x-ray diffraction (XRD) measurements [30], according to which Mn<sub>2</sub>PtSn crystallizes in inverse tetragonal structure with space group I-4m2 and lattice parameters a = b = 4.51 Å and c = 6.08 Å. The 8-atom unit cell is shown in figure 1(a). The initial lattice parameters are set to a = b = 4.51 Å; c = 6.38 Å. Here, the in-plane lattice constants (a, b) are set to our experimental values, while the out-of-plane lattice constant (c)is set to the value corresponding to the cubic supercell (see figure 1(b)), i.e.  $4.51 \text{ Å} = (6.38 \text{ Å})/\sqrt{2}$ . Next, we perform series of calculations for a range of in-plane lattice parameters, for each of which we find the out-of-plane lattice parameter corresponding to the lowest energy. Results are shown in figure 2. One can see that the initial lattice parameters (cubic symmetry) correspond to the highest energy in the considered range, while both compressive and tensile biaxial strain applied to our original cell produce energy minimums, corresponding to distinct tetragonal symmetry.

The calculated lattice parameters corresponding to the two energy minimums are a=4.16 Å, c=7.46 Å (compressive strain of the cubic supercell), and a=4.81, c=5.63 Å (tensile strain of the cubic supercell). The corresponding cla values calculated for the cubic supercell (see figure 2(b)) are 1.27 and 0.83, with the former corresponding to the lowest energy state. These results demonstrate that the bulk Mn<sub>2</sub>PtSn is tetragonal, which is in agreement with recent experimental reports [22, 30]. At the same time, the calculated lattice parameters are different from those obtained recently with XRD measurement [30], which may be due to other reasons, such as different geometry (experimental measurements were performed on thin film samples), atomic disorder, substrate

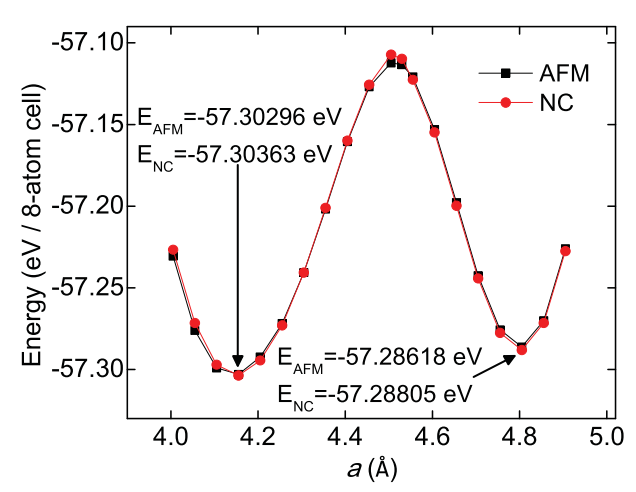


**Figure 4.** Calculated total energies of bulk Mn<sub>2</sub>PtSn, for AFM (black squares) and NC (red spheres) magnetic structures. Total energies corresponding to both energy minimums are shown on the figure.

induced strain, temperature effects, etc. Next, we analyze the behavior of the magnetic structure of Mn<sub>2</sub>PtSn in the considered range of the biaxial strain.

#### 3.2. Magnetic structure

There have been conflicting reports in recent literature regarding the magnetic structure of  $Mn_2PtSn$ . In particular, our recent measurement of magnetization value for  $Mn_2PtSn$  thin film is 5.3  $\mu_B/f.u.$  [30], significantly larger than our early measurements of 3.9  $\mu_B/f.u.$  for bulk  $Mn_2PtSn$  [36]. At the same time, both these values are significantly smaller than the value of 6.7  $\mu_B/f.u.$  predicted by earlier density functional calculations for inverse tetragonal  $Mn_2PtSn$  [37] assuming a collinear arrangement of manganese moments. The collinear arrangement, however, may not necessarily correspond to the

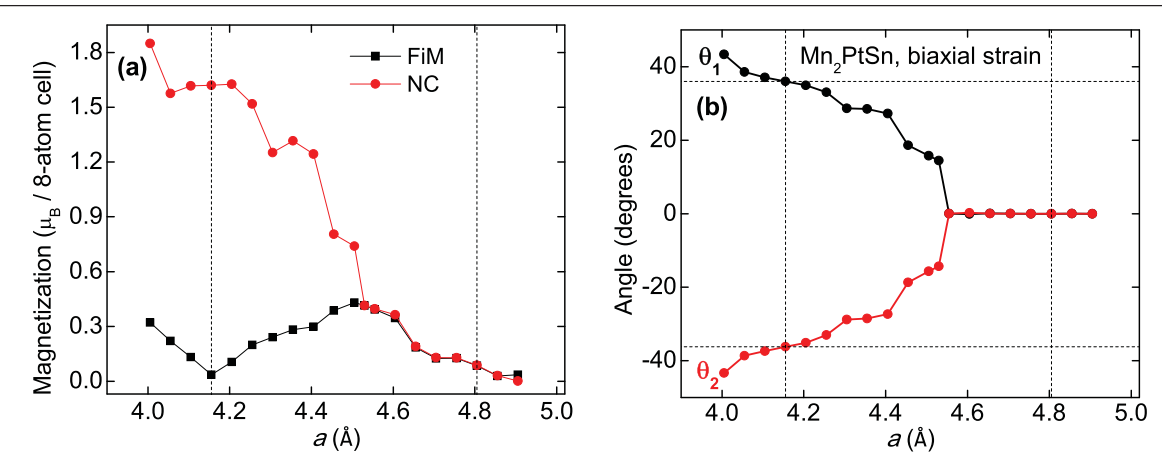


Figure 5. (a) Calculated total magnetic moment, and (b) magnetic moment angles,  $\theta_1$  and  $\theta_2$  (see figure 3(a)) versus in-plane lattice constant of bulk Mn<sub>2</sub>PtSn. Dashed lines indicate energy minimums.

lowest energy state. In particular, it has been recently reported that similar alloys exhibit non-collinear arrangement of magnetic moments [24, 29].

To find the ground state magnetic structure of bulk Mn<sub>2</sub>PtSn, and its modification under biaxial strain, we proceed as follows. For each of the optimized *c/a* ratios (see figure 2), we perform three separate calculations for the following arrangements of magnetic moments: antiferromagnetic (AFM)/ferrimagnetic (FiM), ferromagnetic (FM), and non-collinear (NC). Figure 3 schematically illustrates AFM and NC arrangements in Mn<sub>2</sub>PtSn. For the latter, we choose an initial arrangement of Mn magnetic moments similar to the one reported in [24] for a tetragonal Heusler alloy Mn<sub>2</sub>RhSn. For non-collinear calculations, the magnitudes and directions of local magnetic moments are determined self-consistently for each of the considered *c/a* ratios.

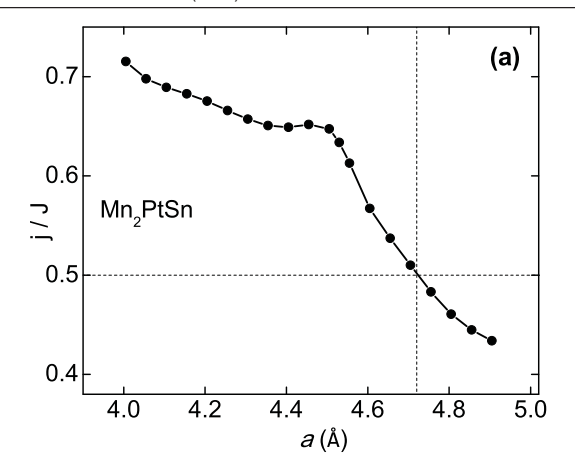
Our calculations indicate that ferromagnetic arrangement corresponds to the highest energy state. In particular, it is more than 0.5 eV/8-atom cell higher than AFM/NC arrangements for the entire range of the considered c/a ratios. This essentially rules out the possibility of ferromagnetic order in zero temperature tetragonal bulk Mn<sub>2</sub>PtSn in the ideal crystal structure (i.e. no atomic disorder, lattice distortions, surface effects, etc). At the same time, AFM and NC arrangements are energetically nearly equivalent, as illustrated in figure 4. For both energy minimums, the non-collinear structure corresponds to a slightly lower total energy, but the energy difference between NC and AFM arrangements is only of the order of  $\approx 1 \text{ meV}$  (see numerical values in figure 4). This probably indicates that at practical temperatures the non-collinear arrangement in ideal bulk Mn<sub>2</sub>PtSn is unstable and undergoes a spin-reorientation transition into antiparallel collinear phase [24], unless it is enhanced by some external stimulus, such as magnetic field and or low dimensional geometry.

Figures 5(a) and (b) correspondingly show calculated total magnetic moments of 8-atom unit cell for antiparallel and non-collinear alignment of Mn moments, and calculated canting angles between c-axis and Mn local magnetic moments,  $\theta_1$  and  $\theta_2$  (see figure 3(a)) of Mn<sub>2</sub>PtSn under biaxial strain. Magnetic moments and canting angles are plotted as a

function of in-plane lattice constant, for optimized c/a ratios. One can see that for the smaller c/a ratios (larger in-plane lattice constant), Mn<sub>2</sub>PtSn is ferrimagnetic, with nearly negligible magnetization. In particular, the non-collinear initial arrangement of the Mn moments relaxes to the antiparallel alignment upon self-consistent calculation, as indicated by zero  $\theta_1$  and  $\theta_2$ angles on the right side of figure 5(b). At  $a = 4.81 \,\text{Å}$  (corresponding to one of the two energy minimums), the calculated total magnetic moment per 8-atom unit cell is  $\approx 0.09 \,\mu_{\rm B}$ . At the same time, for the energy minimum corresponding to the larger c/a ratios (smaller in-plane lattice constant), Mn<sub>2</sub>PtSn can be both AFM/FiM and NC. In other words, the initial NC alignment is preserved upon self-consistent optimization of the magnetic moment directions. Further, since NC and AFM arrangements have nearly identical energies (figure 4), in principle both of these structures are feasible for the larger c/a ratios. Here, at  $a = 4.16 \,\text{Å}$  (corresponding to the energy minimum), the calculated total magnetic moment per 8-atom unit cell is  $\approx 1.62 \,\mu_{\rm B}$  assuming NC arrangement, and  $\approx 0.04 \,\mu_{\rm B}$ assuming antiparallel collinear alignment.

#### 4. Analysis

Typically, the non-collinearity in magnets originates from interplay of parallel and antiparallel exchange interactions. In some cases, e.g. in triangular magnetic systems, this may result in interesting phenomena, such as piezomagnetic [1] and even somewhat exotic flexomagnetic effect, i.e. strain gradient induced magnetization [38]. To analyze the origin of the non-collinear alignment in Mn<sub>2</sub>PtSn, we employ a model suggested by Meshcheriakova et al for a same family material, Mn<sub>2</sub>RhSn [24]. In particular, we consider interplane exchange coupling between nearest (J) and next-nearest (j)planes in c-direction (see figure 3). The latter has to be taken into account to explain non-collinearity, since the nearestplane coupling alone results in collinear (antiparallel in our case) alignment of magnetic moments. At the same time, the next-nearest-plane superexchange coupling along with the nearest-plane exchange results in competing parallel/antiparallel alignments that can lead to the canting of the magnetic



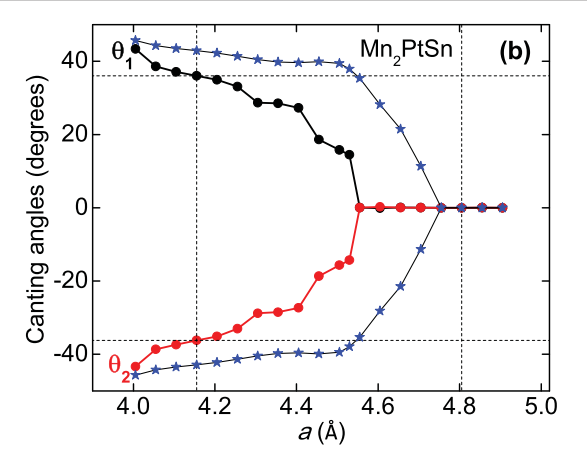


**Figure 6.** (a) Calculated ratio of AFM / FM exchange coupling parameters, j/J, and (b) canting angles,  $\theta_1$  and  $\theta_2$  (see figure 3(a)) versus in-plane lattice constant of bulk Mn<sub>2</sub>PtSn. Blue line and stars correspond to the canting angle calculated theoretically from exchange coupling parameters. Dashed lines indicate energy minimums.

moments [24]. It is shown in [24], that for Mn<sub>2</sub>RhSn one can use the  $\frac{j}{J} > \frac{1}{2}$  condition (i.e. strong next-nearest-plane superexchange) as a criterion of non-collinearity, while the canting angles derived from the spin Hamiltonian are given by  $(\theta)_{1,2} = \pm \arccos\left(\frac{J}{2j}\right)$ . Since Mn<sub>2</sub>RhSn and Mn<sub>2</sub>PtSn belong to the same family of materials, here we use the same conditions to analyze our results. In particular, we employ the following formulas

$$\frac{j}{J} = \frac{|E_{\text{FM}} - E_{\text{NNN,AFM}}|}{|E_{\text{FM}} - E_{\text{NN,AFM}}|}$$

$$(\theta)_{1,2} = \arccos\left(\frac{J}{2j}\right) = \arccos\left(\frac{|E_{\text{FM}} - E_{\text{NN,AFM}}|}{2 \times |E_{\text{FM}} - E_{\text{NNN,AFM}}|}\right).$$

Here,  $E_{\rm FM}$ ,  $E_{\rm NN,AFM}$  and  $E_{\rm NNN,AFM}$  are calculated total energies for ferromagnetic, nearest-plane antiferromagnetic, and next-nearest-plane antiferromagnetic alignments, i.e. NN corresponds to the up/down/up/down, while NNN corresponds to the up/up/down/down arrangements of magnetic moments in c-direction. Figures 6(a) and (b) show calculated  $\frac{j}{J}$  and  $(\theta)_{1,2}$  (blue stars) as a function of in-plane lattice constant, for the entire range of the considered biaxial strain. In figure 6(b), for convenience of comparison, the calculated  $(\theta)_{1,2}$  values are superimposed on the canting angles calculated from self-consistent relaxation of the magnetic moment directions (i.e. figure 5(b)).

As shown in figure 6(a), for smaller in-plane lattice parameters, Mn<sub>2</sub>PtSn satisfies the non-collinearity condition  $\frac{j}{J} > \frac{1}{2}$ , while for larger in-plane lattice constant, this condition breaks down. The transition point is at  $a \approx 4.72\,\text{Å}$ , which is larger but only by  $\approx 0.15\,\text{Å}$  than the value of  $a \approx 4.55\,\text{Å}$  calculated from self-consistent relaxation of atomic moments (see figure 5(b)). The canting angles calculated from  $(\theta)_{1,2} = \arccos\left(\frac{J}{2j}\right)$  (figure 6(b)) show the same  $a \approx 4.72\,\text{Å}$  non-collinear to antiparallel collinear transition point, and are in qualitative agreements with the dynamics of the magnetic moments deduced from

their self-consistent relaxation (compare red/black and blue plots in figure 6(b)). These results confirm that the non-collinearity in Mn<sub>2</sub>PtSn originates from the competition of nearest-and next-nearest-plane exchange couplings, in agreement with the mechanism described in [24]. The small discrepancy of  $a \approx 0.15 \, \text{Å}$  of the non-collinear to collinear transition point is possibly due to the exclusion of the in-plane exchange coupling between Mn atoms from the considered model.

#### 5. Conclusions

Combined effects of tetragonality and non-collinear magnetic order in Mn<sub>2</sub>PtSn Heusler material are studied from first principles. It is demonstrated that this material has two energetically close energy minima corresponding to tetragonal lattice. In one of these phases, Mn<sub>2</sub>PtSn exhibits ferrimagnetic order with nearly fully compensated total magnetic moment, while in the other phase (corresponding to the lowest energy), a non-collinear magnetic arrangement emerges, with very large canting angles of Mn local magnetic moments. The non-collinear alignment is explained through the competition between exchange (favoring antiparallel alignment) and superexchange (favoring non-collinear alignment) couplings between nearest- and next-nearest-plane Mn atoms.

#### **Acknowledgments**

Research at the University of Northern Iowa (UNI) is supported by the UNI Faculty Summer Fellowship. This work used the Extreme Science and Engineering Discovery Environment (XSEDE), which is supported by National Science Foundation grant number ACI-1548562. This work used the XSEDE Regular Memory (Bridges) and Storage (Bridges Pylon) at the Pittsburgh Supercomputing Center (PSC) through allocation TG-DMR180059 [39]. Research at the University of Nebraska is supported by the National Science Foundation under the awards DMREF:SusChEM 1436386 and ECCS: 1542182,

and by the Nebraska Center for Materials and Nanoscience which is supported by the Nebraska Research Initiative.

#### **ORCID iDs**

P V Lukashev https://orcid.org/0000-0002-2551-5954

#### References

- [1] Lukashev P, Sabirianov R F and Belashchenko K 2008 Phys. Rev. B 78 184414
- [2] Tsymbal E Y and Žutic I 2011 (ed) Handbook of Spin Transport and Magnetism (Boca Raton, FL: CRC Press) p 808
- [3] Kent A D, Özyilmaz B and del Barco E 2004 Appl. Phys. Lett. 84 3897
- [4] Lee K J, Redon O and Dieny B 2005 Appl. Phys. Lett. 86 022505
- [5] Mangin S, Ravelosona D, Katine J A, Carey M J, Terris B D and Fullerton E E 2006 Nat. Mater. 5 210
- [6] Chappert C, Fert A and Van Dau F N 2007 Nat. Mater. 6 813
- [7] Tsymbal E Y, Mryasov O N and LeClair P R 2003 J. Phys.: Condens. Matter 15 R109
- [8] Yuasa S 2011 Handbook of Spin Transport and Magnetism ed E Y Tsymbal and I Žutić (Boca Raton, FL: CRC Press) ch 11, p 217
- [9] Belashchenko K D and Tsymbal E Y 2011 Handbook of Spin Transport and Magnetism ed E Y Tsymbal and I Žutić (Boca Raton, FL: CRC Press) ch 12 p 233
- [10] Lukashev P V, Wysocki A L, Velev J P, van Schilfgaarde M, Jaswal S S, Belashchenko K D and Tsymbal E Y 2012 Phys. Rev. B 85 224414
- [11] Johnson M and Silsbee R H 1985 Phys. Rev. Lett. 55 1790
- [12] Žutic I, Fabian J and Das Sarma S 2004 Rev. Mod. Phys. 76 323
- [13] Jedema F J, Filip A T and van Wees B J 2001 Nature 410 345
- [14] Webster P J and Ziebeck K R A 1988 Alloys and Compounds of d-Elements with Main Group Elements. Part 2

- (Landolt-Börnstein, New Series, Group III vol 19c) ed H R J Wijn (Berlin: Springer) p 75
- [15] Kübler J 2003 Phys. Rev. B 67 220403
- [16] Felser C and Hirohata A 2016 Heusler Alloys (Springer Series in Materials Science vol 222) ed I Galanakis (Berlin: Springer)
- [17] Faleev S V, Ferrante Y, Jeong J, Samant M G, Jones B and Parkin S P 2017 Phys. Rev. Appl. 7 034022
- [18] Kanomata T, Sasaki T, Nishihara H, Yoshida H, Kaneko T, Hane S, Goto T, Takeishi N and Ishida S 2005 J. Alloys Compd. 393 26
- [19] Chena X-Q, Podloucky R and Rogl P 2006 J. Appl. Phys. 100 113901
- [20] Oxley D P, Tebble R S, Slack C T and Williams K C 1962 Nature 194 465
- [21] Tas M, Sasioglu E, Friedrich C, Blügel S and Galanakis I 2017 J. Appl. Phys. 121 053903
- [22] Nayak A K et al 2015 Nat. Mater. 14 679
- [23] Jamer M E et al 2017 Phys. Rev. Appl. 7 064036
- [24] Meshcheriakova O et al 2014 Phys. Rev. Lett. 113 087203
- [25] Singh S et al 2016 Nat. Commun. 7 12671
- [26] Baláž P, Gmitra M and Barnas J 2009 Phys. Rev. B 80 174404
- [27] Chung N L, Jalil M B A, Tan S G, Guo J and Kumar S B 2008 J. Appl. Phys. 104 084502
- [28] Soncini A and Chibotaru L F 2010 Phys. Rev. B 81 132403
- [29] Nayak A K, Kumar V, Ma T, Werner P, Pippel E, Sahoo R, Damay F, Rößler U K, Felser C and Parkin S S P 2017 Nature 548 561
- [30] Jin Y, Valloppilly S, Kharel P, Waybright J, Lukashev P, Li X Z and Sellmyer D J 2018 J. Appl. Phys. 124 103903
- [31] Blöchl P 1994 Phys. Rev. B 50 17953
- [32] Kresse G and Joubert D 1999 Phys. Rev. B 59 1758
- [33] Perdew J P, Burke K and Ernzerhof M 1996 Phys. Rev. Lett.
- [34] Methfessel M and Paxton A T 1989 Phys. Rev. B 40 3616
- [35] 2017 MedeA-2.22 (San Diego, CA: Materials Design, Inc.)
- [36] Huh Y, Kharel P, Nelson A, Shah V R, Pereiro J, Manchanda P, Kashyap A, Skomski R and Sellmyer D J 2015 J. Phys.: Condens. Matter 27 076002
- [37] Kübler J and Felser C 2012 Phys. Rev. B 85 012405
- [38] Lukashev P and Sabirianov R F 2010 Phys. Rev. B 82 094417
- [39] Towns J 2014 XSEDE: accelerating scientific discovery Comput. Sci. Eng. 16 62–74